Scientific Reports

https://doi.org/10.1038/s41598-026-40206-1

Article in Press

The matricellular protein CCN5 (WISP2) inhibits cellular senescence in cardiac myoblasts and fibroblasts

Received: 17 September 2025

Accepted: 11 February 2026

Published online: 20 February 2026

Cite this article as: Jo Y., Lee M., Kim S.B. *et al.* The matricellular protein CCN5 (WISP2) inhibits cellular senescence in cardiac myoblasts and fibroblasts. *Sci Rep* (2026). https://doi.org/10.1038/s41598-026-40206-1

Yongjoon Jo, Miyoung Lee, Sung Bin Kim, Tae Hwan Kwak, Dongtak Jeong, Seung Pil Jang & Woo Jin Park

The Matricellular Protein CCN5 (WISP2) inhibits Cellular Senescence in Cardiac Myoblasts and Fibroblasts

Yongjoon Jo[1], Miyoung Lee[1], Sung Bin Kim[1], Tae Hwan Kwak[2], Dongtak Jeong[3], Seung Pil Jang[4] and Woo Jin Park[1]

[1] Department of Life Sciences, Gwangju Institute of Science and Technology (GIST), Gwangju, Republic of Korea

[2] BethphaGen, Gwangju, Republic of Korea

[3] Department of Medicinal & Life Science, College of Science and Convergence Technology, Hanyang University-ERICA, Ansan, Republic of Korea

[4] Center for Gene and Cell Therapy, Korea Research Institute of Bioscience and Biotechnology, Daejeon, Republic of Korea

*Correspondence:
Seung Pil Jang, Moai27@gmail.com
Woo Jin Park, woojinpark@icloud.com

Keywords: CCN5; WISP2; Cellular senescence; H9c2; Cardiac myoblasts; Cardiac fibroblasts

Abstract

Cardiovascular diseases remain the leading cause of global mortality. Cellular senescence has recently been implicated in the pathogenesis of various cardiovascular diseases. Our group has previously shown that the matricellular protein CCN5 is a potent anti-fibrotic molecule capable of inhibiting and reversing cardiac fibrosis. In this study, we investigated whether CCN5 can modulate cellular senescence in the heart utilizing three readouts: western blotting for p53 and p21, staining for senescence-associated β-galactosidase, and microscopic analysis of γH2AX-foci. CCN5 effectively inhibited doxorubicin-induced cellular senescence in both H9c2 cardiac myoblasts and fibroblasts. In addition, CCN5 suppressed cellular senescence in H9c2 cardiac myoblasts induced by the senescence-associated secretory phenotype factors secreted from cardiac fibroblast, and *vice versa*. CCN5 also restored the apoptotic response of senescent cells. Finally, CCN5 attenuated myocardial infarction-induced cellular senescence in mice. Collectively, our findings provide novel insights into the potential role of CCN5 in the development of anti-senescence therapies.

Introduction

Cardiovascular diseases, including cardiomyopathy, arrhythmia, and heart failure, remain a leading cause of global mortality, with their prevalence increasing alongside an aging population[1-3]. Recent studies have shown that cellular senescence is closely linked to the pathogenesis and progression of diverse cardiovascular diseases by driving structural and functional alterations in the myocardium[4-6].

Stress-induced cellular senescence is a fundamental response to diverse insults such as DNA damage, mitochondrial dysfunction, and oncogenic activation. While it initially serves as a rapid protective mechanism, persistent senescence leads to detrimental consequences. Senescent cells are characterized by growth arrest, morphological changes, increased mitochondrial activity, and resistance to apoptotic stimuli. They also display a distinct phenotype known as the senescence-associated secretory phenotype (SASP), defined by the secretion of various cytokines, growth factors, and matrix metalloproteinases[7-9].

In the heart, senescent cells contribute to interstitial fibrosis, chronic inflammation, and extracellular matrix remodeling, thereby driving both diastolic and systolic dysfunction[4-6]. The limited regenerative capacity of the myocardium further exacerbates these age-related changes, increasing vulnerability to stressors such as metabolic overload, hypertension, and ischemic injury. More specifically, senescent cardiac myocytes develop hypertrophy, mitochondrial dysfunction, impaired contractility, and abnormal conduction, ultimately leading to progressive myocardial dysfunction. Senescent cardiac fibroblasts undergo proliferative arrest yet remain metabolically active, characterized by enhanced secretion of SASP-associated factors[10,11].

Two primary strategies have been proposed for targeting senescent cardiac cells. The first employs senolytic drugs to selectively eliminate senescent cells, while the second utilizes senomorphic drugs to suppress deleterious features such as SASP[12,13]. Although various nutritional and pharmacological interventions have been investigated[14-17], their effectiveness in preventing or reversing senescence-associated

pathologies remains limited, underscoring the urgent need for novel therapeutic strategies.

Cell communication network (CCN) proteins (CCN1-6) are matricellular proteins that regulate diverse cellular processes, including fibrosis, angiogenesis, and wound healing. While most CCN proteins contain four distinct domains, IGFBP, vWC, TSP-1, and CT, CCN5 uniquely lacks the CT domain[18,19]. This structural distinction has led to the hypothesis that CCN5 may function as an endogenous inhibitor of other CCN members. Supporting this idea, our group has shown that CCN5 inhibits cardiac hypertrophy and fibrosis, at least in part, by counteracting CCN2 activity[20-22]. Previous studies further demonstrated that CCN1 and CCN2 promote fibroblast senescence[23-26]. Therefore, we hypothesized that CCN5 may regulate cellular senescence by antagonizing CCN1 or CCN2.

In the present study, we investigated the role of CCN5 in cellular senescence using cultured rat cardiac myoblasts and fibroblasts. Our results demonstrated that CCN5 suppressed cellular senescence induced by doxorubicin and by SASP factors in these cells. Moreover, CCN5 attenuated myocardial infarction (MI)-induced cellular senescence in the mouse heart. These findings suggest that CCN5 may serve as a potential therapeutic target for anti-senescence strategies in the heart.

Results

Doxorubicin (Dox) induces cellular senescence in H9c2 cardiac myoblasts and fibroblasts

Doxorubicin (Dox) is known to induce cellular senescence in diverse cell types primarily by eliciting genotoxic stress[27-29]. To establish cellular senescence in cultured rat cardiac myoblasts (H9c2) and cardiac fibroblasts, cells were treated with 100 nM Dox for 24 hours. Senescence was then assessed using three readouts. First, the expression of cell cycle regulators p53 and p21 was evaluated by western blotting. Second, senescent cells were quantified by microscopic detection of senescence-associated (SA) β-galactosidase activity. Third, accumulation of the DNA damage marker γH2AX was examined by immunostaining. All three assays consistently demonstrated that Dox effectively induced cellular senescence in both H9c2s and fibroblasts (Supplementary Fig. 1). Accordingly, this protocol was employed in subsequent experiments to induce cellular senescence *in vitro*.

CCN5 inhibits Dox-induced cellular senescence in H9c2 cardiac myoblasts and fibroblasts

We next examined whether CCN5 modulates Dox-induced cellular senescence in H9c2s. After 24 hours of Dox treatment, the culture medium was replaced with fresh medium, and purified CCN5 protein (500 ng/mL) was added for an additional 24 hours (Fig. 1A). CCN5 treatment reduced the expression levels of p53 and p21 (Fig. 1B), decreased the number of SA-β-galactosidase-positive cells (Fig. 1C), and lowered the number of γH2AX foci compared with untreated cells (Fig. 1D). These results indicate that CCN5 suppresses cellular senescence in H9c2s.

We then performed similar experiments in cardiac fibroblasts (Fig. 2A). As in H9c2s, CCN5 treatment reduced the levels of senescent marker proteins (Fig. 2B), decreased the number of SA-β-galactosidase-positive cells (Fig. 2C), and diminished γH2AX foci (Fig. 2D).

Dox also increased the expression levels of SASP, as assessed by

qPCR, with different profiles across cell types. Importantly, CCN5 treatment significantly inhibited this Dox-induced upregulation of SASP in both cell types (Supplementary Fig. 2).

Oxidative stress is a critical driver of senescence, therefore, we examined whether CCN5 modulates intracellular reactive oxygen species (ROS) levels. Dox increased ROS levels in both H9c2 cells and cardiac fibroblasts, and this increase was markedly attenuated by CCN5 (Supplementary Fig. 3). In addition, CCN5 efficiently suppressed senescence induced by 96 hours of Dox treatment (Supplementary Figure 4).

Together, these findings demonstrated that CCN5 inhibits Dox-induced cellular senescence in both cardiac myoblasts and fibroblasts.

CCN5 inhibits SASP-induced cellular senescence in H9c2 cardiac myoblasts and cardiac fibroblasts

Senescent cells secret diverse factors, including cytokines, growth factors, and matrix metalloproteinases, collectively termed SASP factors. These factors exert paracrine effects that drive neighboring healthy cells into cellular senescence. Previous studies have shown that SASP secreted from H9c2s can induce cellular senescence in adjacent fibroblasts[30,31], and vice versa, thereby synergistically accelerating cellular senescence in the heart.

We first tested whether CCN5 prevents cellular senescence in H9c2s upon the treatment with SASP secreted from cardiac fibroblasts (Fig. 3A). Cardiac fibroblasts were treated with Dox for 24 hours, followed by culture in fresh medium lacking Dox for an additional 24 hours. The resulting conditioned medium, enriched with SASP, was applied to H9c2s in the presence or absence of purified CCN5 protein (500 ng/mL). Conditioned medium containing SASP induced cellular senescence in H9c2s, as evidenced by elevated senescent markers (Fig. 3B), an increased number of SA-β-galactosidase-positive cells (Fig. 3C), and reduced γH2AX foci (Fig. 3D). All these effects were significantly suppressed by CCN5 treatment.

We next performed similar experiments to test whether CCN5 prevents cellular senescence in cardiac fibroblasts exposed to SASP secreted from H9c2s (Fig. 4A). In this setting, SASP secreted from H9c2s induced cellular senescence in cardiac fibroblasts, as shown by all readouts, which was markedly attenuated by CCN5 (Fig. 4B~D).

Collectively, these findings demonstrated that CCN5 inhibits senescence not only induced by Dox but also triggered by SASP secreted from neighboring cardiac cell types.

CCN5 restores apoptotic responses in senescent H9c2 cardiac myoblasts and fibroblasts

Senescent cells are resistant to apoptotic stimuli, and their persistence is particularly detrimental in chronic disease states. We therefore tested whether CCN5 could restore apoptotic responsiveness in H9c2s and fibroblasts. Cells were treated with Dox for 24 hours, followed by purified CCN5 protein for an additional 24 hours, as described above. Apoptosis was then induced by treatment with staurosporine (STS, 100 nM) for 9 hours (Fig. 5A, D)[32].

Western blotting revealed that cleaved PARP (c-PARP) and cleaved caspase 3 (c-Caspase 3) were significantly elevated in non-senescent cells (Cont), but not in Dox-treated senescent cells (Dox). This implies that the senescent H9c2s and fibroblasts are indeed resistant to STS. CCN5 treatment restored sensitivity to STS in both H9c2s and fibroblasts, as indicated by increased c-PARP and c-Caspase 3 levels (Dox+CCN5) (Fig. 5B, E). Consistently, TUNEL assays showed a marked reduction in TUNEL-positive cells in senescent cells (Dox) compared with controls (Cont), which was significantly reversed by CCN5 treatment (Dox+CCN5) (Fig. 5C, F). Together, these findings indicate that CCN5 normalizes the apoptotic response in senescent cardiac myoblasts and fibroblasts.

CCN5 inhibits senescence in an *in vivo* mouse heart model

We have previously shown that short-term expression of CCN5 via direct

intramyocardial injection of modified mRNA encoding CCN5 (ModRNA-CCN5) significantly ameliorates structural and functional deterioration in mouse hearts subjected to myocardial infarction (MI)[33,34]. Using the same model, we investigated whether CCN5 also modulates cellular senescence in the infarcted heart. Coronary artery ligation to induce MI and intramyocardial injection of ModRNA-CCN5 were performed sequentially on the same day. Hearts were harvested on day 7 for molecular and histological analyses (Fig. 6A). The cardioprotective effects of CCN5 were confirmed by fibrotic marker, echocardiography and histological analyses (Supplementary Fig. 5). ModRNA-mediated expression of CCN5 was confirmed by western blotting (Supplementary Fig. 6). MI markedly increased of p53, p21 and p16 expression (Fig. 6B), the area and intensity of SA-β-galactosidase positive cells (Fig. 6C), and the number of γH2AX-foci (Fig. 6D) compared with sham-operated control hearts. CCN5 treatment significantly attenuated all of these cellular senescence-associated changes (Fig. 6B~D). These findings indicate that CCN5 effectively inhibits cellular senescence *in vivo* in mouse heart following MI.

Discussion

This study demonstrates that CCN5 inhibits cellular senescence in H9c2 cardiac myoblasts and fibroblasts induced by Dox, a widely used reagent for senescence induction. We further showed that CCN5 prevents cellular senescence in these cells driven by SASP factors secreted from neighboring cells in a reciprocal manner. SASP-mediated secondary senescence drives a positive feedback loop that accelerates the expansion of senescent cells *in vivo*[5]. The anti-senescent effect of CCN5 was further validated in an *in vivo* model of MI-induced cardiac senescence. Collectively, these findings suggest that CCN5 represent a promising therapeutic target for modulating cellular senescence in the heart.

Other CCN members have been reported to exert context-dependent roles in regulating cellular senescence. For example, CCN1 induces cellular senescence in multiple organs, including the skin, liver, and heart, and in diverse range of cell types, including fibroblasts, chondrocytes, and carcinoma cells[19,20]. CCN2 has been shown to promote cellular senescence in skin fibroblast, which helps to restrict fibrosis during tissue repair[21,22]. Furthermore, CCN1 and CCN3 have been directly implicated in the pathology of osteoarthritis by inducing chondrocyte senescence[35-37].

This study was motivated by our previous findings that CCN5 antagonizes CCN2 activity in both the heart[20,21] and eye[38-40]. CCN2 expression is elevated in failing hearts under various pathological insults and is closely associated with cardiac fibrosis. We previously demonstrated that CCN5 inhibits cardiac fibrosis at least in part by downregulating CCN2. Similarly, CCN2 levels are elevated in the mouse retina under multiple pathogenic conditions and are linked to neovascularization and degeneration of retinal pigmented epithelium. In this contexts as well, CCN5 suppressed retinal pathologies while concomitantly reducing CCN2 expression. Based on these findings, we hypothesized that CCN5 may inhibit cellular senescence in the heart by antagonizing CCN2 and possibly other CCN family members.

Although our data clearly demonstrate that CCN5 inhibits cellular

senescence in the heart, the underlying molecular mechanism remains unclear. For example, CCN2 expression levels were unaltered following treatment with Dox[41] (data not shown). suggesting that suppression of the CCN2 is unlikely to account for the anti-senescence activity of CCN5. We previously showed that CCN5 reverses pre-formed cardiac fibrosis by actively inducing the reverse trans-differentiation of myofibroblasts[19]. By analogy, CCN5 may similarly trigger a reverse process of cellular senescence.

This study is subject to several limitations. First, our experiments relied primarily on H9c2 cardiac myoblasts. Although H9c2 cells are a well-established cardiac model, validation using human iPSC-derived cardiac myocytes is warranted to fully establish the translational relevance of these findings to cardiac myocytes. Second, regarding the mechanisms of senescence, while p16 is an important senescence marker, our *in vitro* Dox model demonstrated that p16 levels were not significantly altered by CCN5 treatment, despite being upregulated by Dox (Supplementary Data 1). In contrast, a rapid downregulation of p21 mRNA was observed within 3 hours of CCN5 administration. These data suggest that in the context of Dox-induced senescence, CCN5 likely mediates its effects predominantly via the p53/p21 axis rather than the p16 pathway. Notably, our unpublished observations in a TGF-β induced senescence model indicated p16 regulation by CCN5, suggesting that the molecular targets of CCN5 are context-dependent.

Given that CCN5 modulates cellular senescence induced by Dox and SASP, it may serve as a senomorphic strategy by preventing the onset of senescence. Moreover, through its ability to restore apoptotic sensitivity in senescent cells, CCN5 may also function as a senolytic strategy, promoting the removal of existing senescent cells.

Overall, this study elucidates an anti-senescent function CCN5 in the heart. Together with its previously identified anti-fibrotic activity, these findings position CCN5 as a promising therapeutic modality for a broad spectrum of heart diseases.

Methods

Cells and cell culture

Rat cardiac fibroblasts (RCF), adult (Cell Applications, R306-05a) were cultured in FGM medium (Cell Applications). H9c2 cells were cultured in High-Glucose DMEM (HyClone, Cytiva) at 37°C in a 5% CO_2 incubator. HEK 293-F cells (Gibco, #R79007) were suspension-cultured in Freestyle 293 medium (Gibco, #12338018) at 37°C in an 8% CO_2 incubator with continuous shaking.

Purification of recombinant proteins

cDNAs encoding the full-length human CCN5 protein were subcloned into a pcDNA3.1-myc-his plasmid and subsequently transfected into HEK 293-F cells. One day prior to transfection, 1 x 10^6cells were seeded into Freestyle 293 medium. On the day of transfection, plasmid DNA was diluted in Opti-MEM medium (Gibco, #51985034). FectoPRO transfection reagent (Polyplus, #116–001) was then added to the diluted plasmid DNA at a 1:1 ratio, and the mixture was incubated for 10 minutes at room temperature. The mixture was added to the cultured HEK 293-F cells. Three days' post-transfection, the culture medium was collected and centrifuged at 2,000 × g for 10minutes. Proteins from the culture medium were purified using Capturem His-Tagged Purification Maxiprep Columns (Takara, #635715). The purified proteins were stored in a buffer containing 20 mM $NaHPO_4$, 150 mM NaCl, and 250 mM imidazole at -70°C[42].

Induction of senescence, CCN5 treatment, and SASP-containing media preparation

Senescence was induced by administering doxorubicin (100 nM) to cells in growth media for 24 hours. Purified CCN5 protein (500 ng/ml) was added to cells for 24 hours in media containing 0.1% FBS. Staurosporine (100 nM) was applied to cells after CCN5 treatment for 9hours. To test SASP, following 24 hours of Dox treatment and a single wash with PBS, the

medium was replaced with growth medium containing 0.1% FBS to remove Dox. Cells were then incubated for 24 hours to generate SASP-containing conditioned media (CM). CM were treated with CCN5 protein for 24 hours. For long-term senescence assays, H9c2 cells were treated with Dox (100 nM) for 4 days. The culture medium containing Dox was refreshed every 48 hours.

Western blotting

Cell lysates were solubilized in RIPA buffer (50 mM Tris, 150 mM NaCl, 0.1% SDS, 1% Triton X-100, pH 8.0) supplemented with Protease Inhibitor Cocktail Set III (Merck Millipore, #535140). Cell lysates were quantified using a Pierce BCA Protein Assay Kit (Thermo Scientific, #23227), separated by sodium dodecyl sulfate-polyacrylamide gel electrophoresis (SDS-PAGE), and then transferred to polyvinylidene difluoride (PVDF) membranes (Merck Millipore, #IPVH00010). Blots were blocked with a 3% BSA solution and incubated with primary antibodies against p53(Abcam), p21(Abcam), p16 (Santa Cruz, sc-1661), p16 (Abcam, #ab32072), GAPDH (CST), beta-actin (Santa Cruz), PARP(CST), caspase3(CST) and cleaved-caspase3(CST) for 12–16 hours at 4°C. After washing with Tris-buffered saline containing 0.1% Tween 20 (TBS-T), blots were incubated with horseradish peroxidase (HRP)-conjugated secondary antibodies (Thermo Scientific, #31460 for rabbit, #31430 for mouse), and washed again. Signals were developed using a EZ-Western Lumi Pico Kit (Dogenbio, Seoul, Korea) and Western Femto ECL Kit (FEMTO-100) and were detected by Amersham™ ImageQuant™ 800 (Cytiva).

Senescence-associated β-galactosidase (SA-β-gal) assay

SA-β-gal assay was assessed according to the manufacturer's protocol (CST #9860). For *in vitro* SA-β-gal assay, fibroblasts and H9c2s were seeded on 6-well plates. Fluorescence microscopy and DIC images were captured from random fields in each well using an EVOS M7000. SA-β-gal positive cells are normalized against Hoechst-positive nucleus. For *in vivo*

SA-β-gal assay, frozen heart tissues were outlined with ImmEdge® Hydrophobic Barrier PAP Pen (H-4000) and soaked in SA-β-gal staining solution. Fluorescence microscopy and DIC images were captured using Olympus research slide scanner. All assays were performed in at least triplicate, with at least 300-500 cells counted per sample from randomly selected fields. SA-β-gal signals were analyzed using ImageJ 1.53 (https://imagej.net/ij/) software. The same settings (threshold, color threshold, brightness, analyze particles) were applied for each experimental set. Color Thresholding was applied to selectively retain the blue-colored SA-β-gal stained regions. Thresholding process was employed to eliminate background noise, enabling the accurate determination and analysis of both nuclei and the SA-β-gal-stained areas.

Immunocytochemistry

Cells were seeded onto 16 mm coverslips. After CCN5 treatment, cells were fixed with 4% PFA, permeabilized with 0.2% Triton X-100, and blocked with a 5% BSA solution. Subsequently, cells were incubated with a primary antibody against γH2AX (JBW301, Merck), followed by incubation with Alexa Fluor 488 (Invitrogen, A11008) conjugated secondary antibodies. Hoechst 33342 dye was used for nuclear staining. Fluorescence microscopy images were captured using an Olympus fluorescent microscope. All assays were performed in at least triplicate, with at least 100 cells counted per sample from randomly selected fields. Immunofluorescence signals were analyzed using ImageJ software, applying the same settings (threshold, Gaussian distribution, analyze particles) for each experiment set. A Gaussian distribution-based image subtraction was applied to remove noise and extract foci. A thresholding process was also employed to eliminate background noise, enabling the accurate quantification and analysis of both nuclei and the γH2AX foci.

Quantitative Real-Time PCR (qPCR)

Total RNA was extracted from H9c2 cells and cardiac fibroblasts using

TRIzol Reagent. Subsequently, cDNA was synthesized from 1 µg of RNA using a reverse transcriptase (Invitrogen). Quantitative real-time PCR (qPCR) was performed using TB Green® Premix Ex Taq™ (Takara Bio) on a Takara Thermal Cycler Dice™ Real Time System (Takara Bio). Relative gene expression levels were analyzed using the comparative ΔCt method ($2^{-\Delta\Delta Ct}$) and normalized to the internal control (18srRNA).

Measurement of intracellular ROS

Intracellular ROS levels were detected using CellROX™ Green Reagent (Invitrogen). For cardiac fibroblasts, cells were treated with Dox (100 nM) for 24 hours. CCN5 protein (500 ng/ml) was added to cells for 24 hours. For H9c2 cells, cells were treated with Dox (100 nM) for 48 hours. CCN5 protein was added to cells for 24 hours in complete medium containing 10% FBS. Following CCN5 treatment, cells were stained with CellROX Green (5 µm) for 30 minutes at 37°C, and fluorescence intensity was quantified using Microscopy images.

TUNEL assay

TUNEL assay was performed according to the manufacturer's instructions (DeadEnd Fluorometric TUNEL System (Promega, San Luis Obispo, CA, USA). The slides with seeded cells were treated with a TUNEL reaction mixture containing terminal deoxynucleotidyl transferase (TdT) and fluorescein UTP. The reaction was carried out in a humidified chamber at 37 ◦C for 1 hour. After the reaction, the slides were stained with Hoechst 33342 and examined under a fluorescent microscope (Olympus). Apoptotic signals and nuclear signals were counted using ImageJ software with a fixed threshold for each experiment, and the percentage of TUNEL-positive cells was calculated.

Animal experiments and myocardial infarction model

All animal experimental procedures were approved by the Institutional Animal Care and Use Committees of Gwangju Institute of Science and

Technology (GIST). All procedures were conducted in accordance with relevant guidelines and regulations for laboratory animals. This study is reported in accordance with ARRIVE guidelines. C57BL/6 mice (10–12-week-old males, 25–28 g body weight) were obtained from DBL Inc. (Eumseong, Korea). All efforts were made to minimize animal suffering. All mice were housed in an equipped animal facility with temperature of 18-23 °C and humidity at 40-60%, under 12 hours light/dark cycle, and had free access to food and water. To induce myocardial infarction model, mice were anesthetized by a mixture of 95 mg/kg ketamine (Yuhan, Korea) and 5 mg/kg xylazine (Bayer, Germany). The left side of the chest was shaved, and an intubation tube was inserted into the trachea. An incision was made in the fourth intercostal space, and the muscles were separated with scissors. The pericardium was gently removed. Myocardial infarction (MI) was induced by ligation of the left anterior descending (LAD) artery using a 7-0 black silk suture. The chest was sutured with 4-0 black silk. The same surgical procedure, without LAD ligation, was performed for the sham operation. Seven days post-surgery, isoflurane was used for anesthetization via inhalation before euthanasia. Mice were euthanized by cervical dislocation humanely performed by trained researchers in accordance with approved protocols. Harvested hearts were used for western blotting, senescence-associated β-galactosidase (SA-β-gal) assay, and immunohistochemistry.

Cardiac function was evaluated post-MI induction using transthoracic echocardiography (GE Healthcare) to determine the percentage of fractional shortening (FS) and ejection fraction (EF). For histological examination, murine cardiac tissues were sectioned at a thickness of 6 μm. To evaluate fibrotic changes, sections were stained with Masson’s trichrome (Sigma, HT15). For hematoxylin and eosin (H&E) staining, sections were incubated in hematoxylin (26041-06, Electron Microscopy Science, Hatfield) for 30 s, followed by a 10 min wash in running tap water. Subsequently, the sections were counterstained with eosin (EOYA-05-OT-1L, Biognost, Zagreb) for 2 min to visualize the cytoplasm.

Production of modified mRNA-CCN5 and injection

Polyadenylated and capped (CleanCap™ technology) modified RNAs (ModRNAs) were synthesized by TriLink Biotechnologies (San Diego, CA, USA) with full substitution of uridine with pseudo-uridine. The 5′ and 3′ untranslated regions (UTRs) were designed by the Zangi lab (New York, NY, USA). ModRNAs and Lipofectamine RNAiMAX transfection reagent (Invitrogen, Waltham, MA, USA, #13778150) were separately diluted in Opti-MEM, mixed, and incubated for 15 minutes at room temperature. A total of 50 µg of the ModRNA mixture was directly injected into the endocardium adjacent to the infarcted area.

Histology and immunohistochemistry

Harvested tissue samples were fixed in 4% paraformaldehyde for 72 hours at 4°C and incubated in 30% sucrose for 72 hours at 4°C as a cryoprotectant. The tissues were embedded in OCT compound (3801480, Leica, Germany). Frozen tissue blocks were sectioned at 8 µm thickness using a cryostat microtome (HM525NX, Thermo Scientific, USA). Sections were mounted on adhesive slides (J1800AMNZ, Epredia). For γH2AX, immunohistochemistry was performed, which included antigen retrieval by boiling in a pH 6 citrate buffer. Primary antibodies (JBW301, Merck, 1:250) were diluted in a 3% bovine serum albumin blocking solution and applied for incubation. Secondary Alexa Fluor 594 (Invitrogen, A11032) conjugated antibodies were then applied and visualized. Images were acquired using Olympus confocal microscopy (Olympus, Japan). Immunofluorescence signals were analyzed using ImageJ software applying the same settings (threshold, Gaussian distribution, analyze particles) for each experiment set. A Gaussian distribution-based image subtraction was applied to remove noise and extract foci. A thresholding process was employed to eliminate background noise, enabling the accurate quantification and analysis of both nuclei and the γH2AX foci.

Statistical analysis

N numbers represent independent biological observations. All experiments were repeated independently at least three times. One-Way Analysis of Variance (ANOVA) was employed for statistical analyses to determine the significance of the data using Prism10 (GraphPad Software, La Jolla, CA, USA, https://www.graphpad.com). An asterisk (*, $p \leq 0.05$) or a double asterisk (**, $p \leq 0.01$) indicates statistical significance. Data are presented as the mean ± standard deviation.

References

1. Martin, S. S. *et al.* 2025 Heart Disease and Stroke Statistics: A report of US and global data from the American Heart Association. *Circulation* (2025) doi:10.1161/ cir.0000000000001303.
2. Beghini, A. *et al.* 2024 update in heart failure. *ESC Heart Failure* (2024) doi:10.1002/ ehf2.14857.
3. World Health Organization: WHO Cardiovascular diseases (CVDs). https://www.who.int/news-room/fact-sheets/detail/cardiovascular-diseases-(cvds) (2025).
4. Luan, Y. *et al.* Cardiac cell senescence: molecular mechanisms, key proteins and therapeutic targets. *Cell Death Discovery* **10**, (2024).
5. Grootaert, M. O. J. Cell senescence in cardiometabolic diseases. *Npj Aging* **10**, (2024).
6. Evangelou, K. *et al.* Cellular senescence and cardiovascular diseases: moving to the “heart” of the problem. *Physiological Reviews* **103**, 609–647 (2022).
7. González-Gualda, E., Baker, A. G., Fruk, L. & Muñoz-Espín, D. A guide to assessing cellular senescencein vitroandin vivo. *FEBS Journal* **288**, 56–80 (2020).
8. Gorgoulis, V. *et al.* Cellular senescence: defining a path forward. *Cell* **179**, 813–827 (2019).
9. Kumari, R. & Jat, P. Mechanisms of cellular senescence: cell cycle arrest and senescence associated secretory phenotype. *Frontiers in Cell and Developmental Biology* **9**, (2021).
10. Shimizu, I. & Minamino, T. Cellular senescence in cardiac diseases. *Journal of Cardiology* **74**, 313–319 (2019).
11. Zhao, S., Zhang, Y., Zhao, Y. & Lu, X. Cellular senescence as a key player in Chronic heart failure pathogenesis: unraveling mechanisms and therapeutic opportunities. *Progress in Biophysics and Molecular Biology* (2025) doi:10.1016/j.pbiomolbio.2025.02.002.

12. Stojanović, S. D., Thum, T. & Bauersachs, J. Anti-senescence therapies: a new concept to address cardiovascular disease. *Cardiovascular Research* (2025) doi:10.1093/cvr/cvaf030.
13. Suda, M., Katsuumi, G., Tchkonia, T., Kirkland, J. L. & Minamino, T. Potential clinical implications of senotherapies for cardiovascular disease. *Circulation Journal* **88**, 277–284 (2023).
14. Xia, W. *et al.* Depletion of SASP senescent cardiomyocytes with senolytic drugs confers therapeutic effects in doxorubicin-related cardiotoxicity. *FEBS Journal* (2024) doi:10.1111/febs.17164.
15. Scalise, M. *et al.* Senolytics rejuvenate aging cardiomyopathy in human cardiac organoids. *Mechanisms of Ageing and Development* 112007 (2024) doi:10.1016/j.mad.2024.112007.
16. Salerno, N. *et al.* Pharmacological clearance of senescent cells improves cardiac remodeling and function after myocardial infarction in female aged mice. *Mechanisms of Ageing and Development* **208**, 111740 (2022).
17. Yang, B. et al. Ruxolitinib-based senomorphic therapy mitigates cardiomyocyte senescence in septic cardiomyopathy by inhibiting the JAK2/STAT3 signaling pathway. International Journal of Biological Sciences 20, 4314–4340 (2024).
18. Monsen, V. T. & Attramadal, H. Structural insights into regulation of CCN protein activities and functions. *Journal of Cell Communication and Signaling* **17**, 371–390 (2023).
19. Chen, C.-C. & Lau, L. F. Functions and mechanisms of action of CCN matricellular proteins. *The International Journal of Biochemistry & Cell Biology* **41**, 771–783 (2008).
20. Jeong, D. *et al.* Matricellular protein CCN5 reverses established cardiac fibrosis. *Journal of the American College of Cardiology* **67**, 1556–1568 (2016).
21. Yoon, P. O. *et al.* The opposing effects of CCN2 and CCN5 on the development of cardiac hypertrophy and fibrosis. *Journal of Molecular and Cellular Cardiology* **49**, 294–303 (2010).

22. Zhang, L., Li, Y., Liang, C. & Yang, W. CCN5 overexpression inhibits profibrotic phenotypes via the PI3K/Akt signaling pathway in lung fibroblasts isolated from patients with idiopathic pulmonary fibrosis and in an in vivo model of lung fibrosis. *International Journal of Molecular Medicine* **33**, 478–486 (2013).
23. Feng, T. *et al.* CCN1-Induced cellular senescence promotes heart regeneration. *Circulation* **139**, 2495–2498 (2019).
24. Jun, J.-I. & Lau, L. F. The matricellular protein CCN1 induces fibroblast senescence and restricts fibrosis in cutaneous wound healing. *Nature Cell Biology* **12**, 676–685 (2010).
25. Jun, J.-I. & Lau, L. F. CCN2 induces cellular senescence in fibroblasts. *Journal of Cell Communication and Signaling* **11**, 15–23 (2016).
26. Tejedor-Santamaria, L. *et al.* CCN2 activates cellular senescence leading to kidney fibrosis in folic Acid-Induced experimental nephropathy. *International Journal of Molecular Sciences* **26**, 4401 (2025).
27. Von Hoff, D. D. Risk factors for doxorubicin-lnduced congestive heart failure. *Annals of Internal Medicine* **91**, 710 (1979).
28. Maejima, Y., Adachi, S., Ito, H., Hirao, K. & Isobe, M. Induction of premature senescence in cardiomyocytes by doxorubicin as a novel mechanism of myocardial damage. *Aging Cell* **7**, 125–136 (2007).
29. Spallarossa, P. *et al.* Doxorubicin induces senescence or apoptosis in rat neonatal cardiomyocytes by regulating the expression levels of the telomere binding factors 1 and 2. *AJP Heart and Circulatory Physiology* **297**, H2169–H2181 (2009).
30. Tang, X., Li, P.-H. & Chen, H.-Z. Cardiomyocyte senescence and cellular communications within myocardial microenvironments. *Frontiers in Endocrinology* **11**, (2020).
31. Lewis-McDougall, F. C. *et al.* Aged-senescent cells contribute to impaired heart regeneration. *Aging Cell* **18**, (2019).

32. Kato, K. *et al.* Impaired myofibroblast dedifferentiation contributes to nonresolving fibrosis in aging. *American Journal of Respiratory Cell and Molecular Biology* **62**, 633–644 (2020).
33. Magadum, A. *et al.* Specific Modified mRNA translation System. *Circulation* **142**, 2485–2488 (2020).
34. Song, M. H. *et al.* Modified mRNA-Mediated CCN5 Gene Transfer Ameliorates Cardiac Dysfunction and Fibrosis without Adverse Structural Remodeling. *International Journal of Molecular Sciences* **25**, 6262 (2024).
35. Feng, M. *et al.* Inhibition of cellular communication network factor 1 (CCN1)-driven senescence slows down cartilage inflammaging and osteoarthritis. *Bone* **139**, 115522 (2020).
36. Kuwahara, M. *et al.* CCN3 (NOV) drives degradative changes in aging articular cartilage. *International Journal of Molecular Sciences* **21**, 7556 (2020).
37. Fujita, M., Sasada, M., Iyoda, T. & Fukai, F. Involvement of matricellular proteins in cellular senescence: Potential therapeutic targets for Age-Related Diseases. *International Journal of Molecular Sciences* **25**, 6591 (2024).
38. Im, S., Song, M. H., Elangovan, M., Woo, K. M. & Park, W. J. The matricellular protein CCN5 prevents anti-VEGF drug-induced epithelial-mesenchymal transition of retinal pigment epithelium. *Scientific Reports* **14**, (2024).
39. Yoon, A. *et al.* The matricellular protein CCN5 inhibits fibrotic deformation of retinal pigment epithelium. *PLoS One* **13**, e0208897, doi:10.1371/journal.pone.0208897 (2018).
40. Im, S. *et al.* Suppression of choroidal neovascularization and epithelial-mesenchymal transition in retinal pigmented epithelium by adeno-associated virus-mediated overexpression of CCN5 in mice. *PLoS One* **17**, e0269937, doi:10.1371/journal.pone.0269937 (2022).

41. Patricelli, C., Lehmann, P., Oxford, J. T. & Pu, X. Doxorubicin-induced modulation of TGF-β signaling cascade in mouse fibroblasts: insights into cardiotoxicity mechanisms. *Scientific Reports* **13**, (2023).
42. Song, M. H. *et al.* The TSP-1 domain of the matricellular protein CCN5 is essential for its nuclear localization and anti-fibrotic function. *PLoS ONE* **17**, e0267629 (2022).

Acknowledgments

We thank Dr. YS. Oh (Central Research Facility of Gwangju Institute of Science and Technology) for technical assistance of the confocal microscopy. Figures 1 A, 2 A, 3 A, 4 A, 5A and 5D were created with BioRender.com. (https://www.biorender.com, https://BioRender.com/w1x0kdx). During the preparation of this manuscript, the authors used ChatGPT (version 5.0) to assist with proofreading and improving the readability of the manuscript. All content was reviewed and edited by the authors, who take full responsibility for the final version of the publication.

Author contributions statement

Conceptualization, S.P.J. and W.J.P.; methodology, Y.J.J. and M.Y.L.; validation, S.B.K., Y.J.J. and M.Y.L.; formal analysis, Y.J.J.; investigation, Y.J.J.; data curation, S.B.K. and S.P.J.; writing—original draft preparation, Y.J.J.; writing—review and editing, Y.J.J., S.P.J. and W.J.P.; supervision, S.P.J. and W.J.P.; Resources, T.H.K. and D.T.J.; project administration, W.J.P.; funding acquisition, W.J.P.

Funding

This study was supported by funding from the Korea–US Collaborative Research Fund (RS-2024-00466906), the Korea Research Institute of Bioscience and Biotechnology (KRIBB) Research Initiative Program (KGM5362521) and National Research Council of Science & Technology (NST) grant by the Korea government (MSIT) (GTL24022-000)

Competing interests

No potential conflicts of interest exist for other authors.

Data availability statement

All relevant data are within this paper and its Supporting Information files. The datasets used or analyzed during this study are available from the

corresponding authors upon reasonable request.

Figure legends

Fig. 1. CCN5 inhibits Dox-induced cellular senescence in H9c2 cardiac myoblasts.

(A) An experimental scheme is shown (created using Biorender). (B) H9c2s were treated with Dox, followed by CCN5 treatment. Cell lysates were immunoblotted for senescence marker proteins p53 and p21. Protein levels were quantified and normalized to GAPDH (n=4). Panel B is a composite from separate blots for clarity. The uncropped blots are presented in Supplementary Fig. 7. (C) H9c2 cells were stained for SA-β-gal activity. Positive cells were counted in random fields and plotted as a percentages of total cell number (n=3) (D) H9c2 cells were immunostained with antibodies against γH2AX (green) and counter-stained with Hoechst (blue). γH2AX foci were counted in random fields and plotted as a percentage of total nuclei (n=3) (Original magnification, 200x (20x objective)). Scale bar: 50 μm. Data are shown as the mean ± SD. (one-way ANOVA; *$p < 0.05$, **$p < 0.01$).

Fig. 2. CCN5 inhibits Dox-induced cellular senescence in cardiac fibroblasts.

(A) An experimental scheme is shown (created using Biorender). (B) Cardiac fibroblasts were treated with Dox, followed by CCN5 treatment. Cell lysates were immunoblotted for senescence marker proteins p53 and p21. Protein levels were quantified and normalized to GAPDH (n=4). Panel B is a composite from separate blots for clarity. The uncropped blots are presented in Supplementary Fig. 7. (C) Cardiac fibroblasts were stained for SA-β-gal activity. Positive cells were counted in random fields and plotted as a percentages of total cell number (n=3) (D) Cardiac fibroblasts were immunostained with antibodies against γH2AX (green) and counter-stained with Hoechst (blue). γH2AX foci were counted in random fields and plotted as a percentage of total nuclei (Original magnification, 200x (20x objective)) (n=3). Scale bar: 50 μm. Data are shown as the mean ± SD. (one-way ANOVA; *$p < 0.05$, **$p < 0.01$).

Fig. 3. CCN5 inhibits cellular senescence of H9c2 cardiac myoblasts induced by SASP from fibroblasts.

(A) An experimental scheme is shown (created using Biorender). (B) H9c2 were treated with Dox-media or CCN5. Cell lysates were immunoblotted for senescence marker proteins p53 and p21. Protein levels were quantified and normalized to GAPDH (n=4). Panel B is a composite from separate blots for clarity. The uncropped blots are presented in Supplementary Fig. 7. (C) H9c2 cells were stained for SA-β-gal activity. Positive cells were counted in random fields and plotted as a percentages of total cell number (n=3~4) (D) H9c2 cells were immunostained with antibodies against γH2AX (green) and counter-stained with Hoechst (blue). γH2AX foci were counted in random fields and plotted as a percentage of total nuclei (n=3). (Original magnification, 200x (20x objective)) Scale bar: 50 μm. Data are shown as the mean ± SD. (one-way ANOVA; *p < 0.05, **p < 0.01). Dox-media = Doxorubicin treated and SASP-containing conditioned medium

Fig. 4. CCN5 inhibits cellular senescence of cardiac fibroblasts induced by SASP from H9c2 cardiac myoblasts.

(A) An experimental scheme is shown (created using Biorender). (B) Cardiac fibroblasts were treated with Dox-media or CCN5. Cell lysates were immunoblotted for senescence marker proteins p53 and p21. Protein levels were quantified and normalized to GAPDH (n=4). Panel B is a composite from separate blots for clarity. The uncropped blots are presented in Supplementary Fig. 7. (C) Cardiac fibroblasts were stained for SA-β-gal activity. Positive cells were counted in random fields and plotted as a percentages of total cell number (n=3) (D) Cardiac fibroblasts were immunostained with antibodies against γH2AX (green) and counter-stained with Hoechst (blue). γH2AX foci were counted in random fields and plotted as a percentage of total nuclei (n=3). (Original magnification, 200x (20x objective)) Scale bar: 50 μm. Data are shown as the mean ± SD. (one-way ANOVA; *p < 0.05, **p < 0.01). Dox-media = Doxorubicin treated and SASP-containing conditioned medium

Fig. 5. CCN5 restores apoptotic responses in senescent H9c2 cardiac myoblasts and fibroblasts.
(A) An experimental schema is shown for B and C (created using Biorender). (B) H9c2 cardiac myoblasts were treated with Dox, followed by CCN5 treatment and then STS. Cell lysates were immunoblotted for apoptosis marker proteins c-PARP and c-caspase3. Protein levels were quantified and normalized to GAPDH (n=4~7). Panel B is a composite from separate blots for clarity. The uncropped blots are presented in Supplementary Fig. 7. (C) H9c2 were stained for TUNEL assay; TUNEL positive cells were counted in random fields and plotted as percentages of total cell number (N=3) (Original magnification, 200x (20x objective)). (D) An experimental schema is shown for E and F (created using Biorender). (E) Cardiac fibroblasts were treated with Dox, followed by CCN5 treatment and then STS. Cell lysates were immunoblotted for apoptosis marker proteins c-PARP and c-caspase3. Protein levels were quantified and normalized to GAPDH (n=4~7). Panel E is a composite from separate blots for clarity. The uncropped blots are presented in Supplementary Fig. 7. (F) Cardiac fibroblasts were stained for TUNEL assay; TUNEL positive cells were counted in random fields and plotted as percentages of total cell number (N=3) (Original magnification, 200x (20x objective)). Scale bar: 50 μm. Data are shown as the mean ± SD. (one-way ANOVA; *$p < 0.05$, **$p < 0.01$).

Fig. 6. CCN5 inhibits senescence in an *in vivo* mouse heart model.
(A) An experimental scheme is shown (created using Biorender). (B) Heart extract was immunoblotted for senescence marker proteins p53, p21 and p16. Protein levels were quantified and normalized to GAPDH (n=7). Panel B is a composite from separate blots for clarity. The uncropped blots are presented in Supplementary Fig. 7. (C) Heart sections were stained for SA-β-gal activity. Positive cells were counted in random fields and plotted as a percentages of total cell number (n=5) (D) Heart sections were immunostained with antibodies against γH2AX (purple) and counter-

stained with Hoechst (blue). γH2AX foci were counted in random fields and plotted as a percentage of total nuclei (n=4) (Original magnification, 1000x (100x objective)). Scale bar: 50 μm (500μm for 2x images). Data are shown as the mean ± SD. (one-way ANOVA; *$p < 0.05$, **$p < 0.01$).

Fig. 1. CCN5 inhibits Dox-induced cellular senescence in H9c2 cardiac myoblasts.

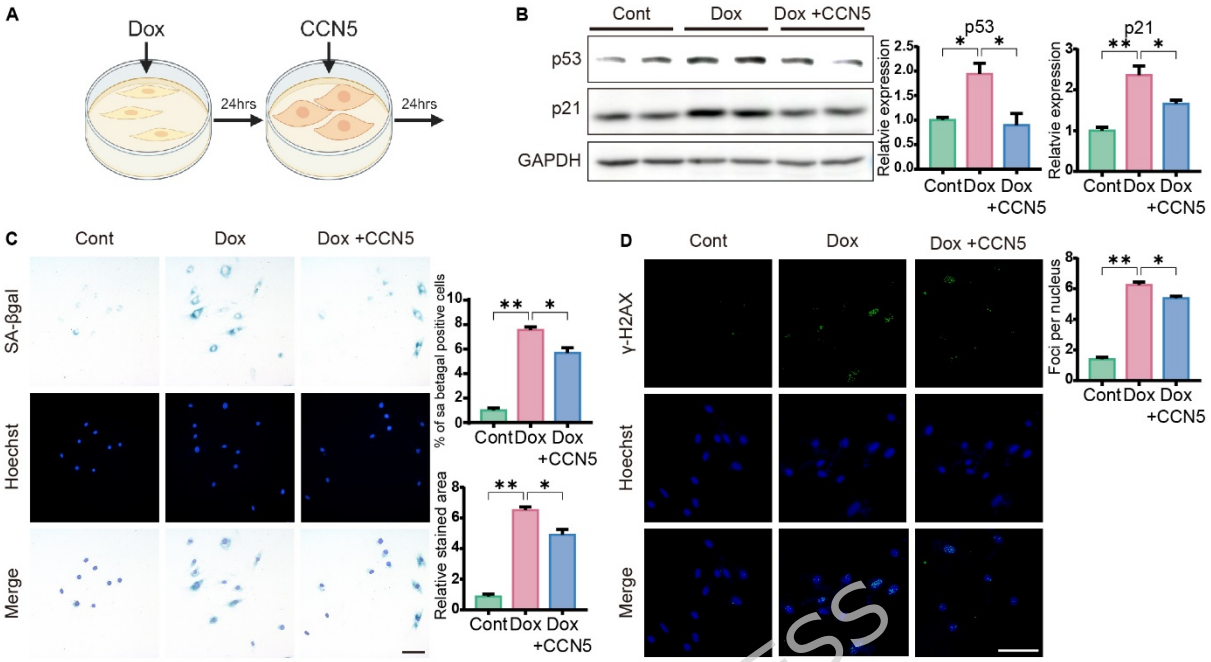

Fig. 2. CCN5 inhibits Dox-induced cellular senescence in cardiac fibroblasts.

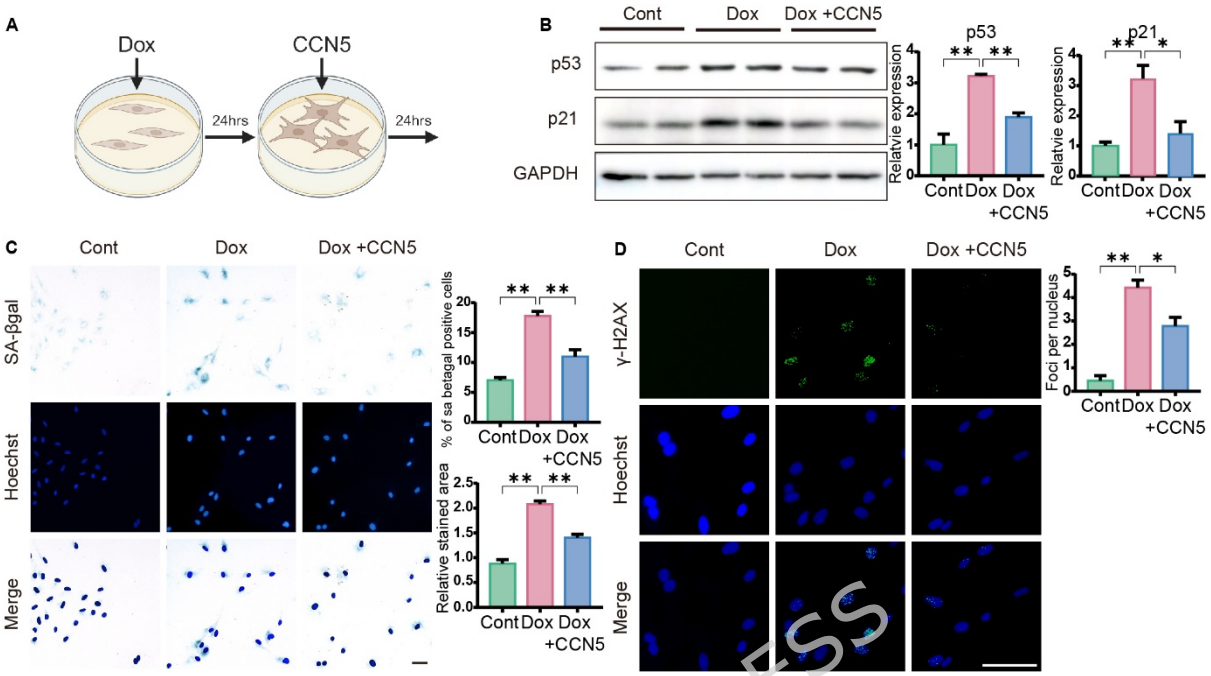

Fig. 3. CCN5 inhibits cellular senescence of H9c2s cardiac myoblasts induced by SASP from fibroblasts.

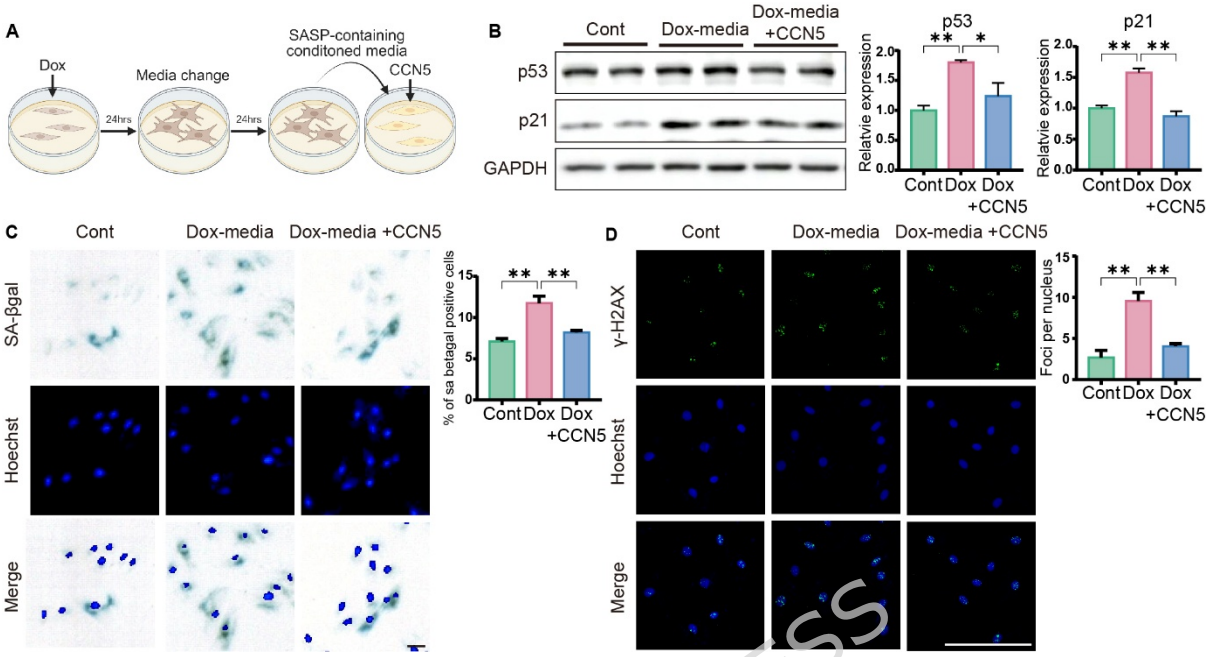

Fig. 4. CCN5 inhibits cellular senescence of cardiac fibroblasts induced by SASP from H9c2 cardiac myoblasts.

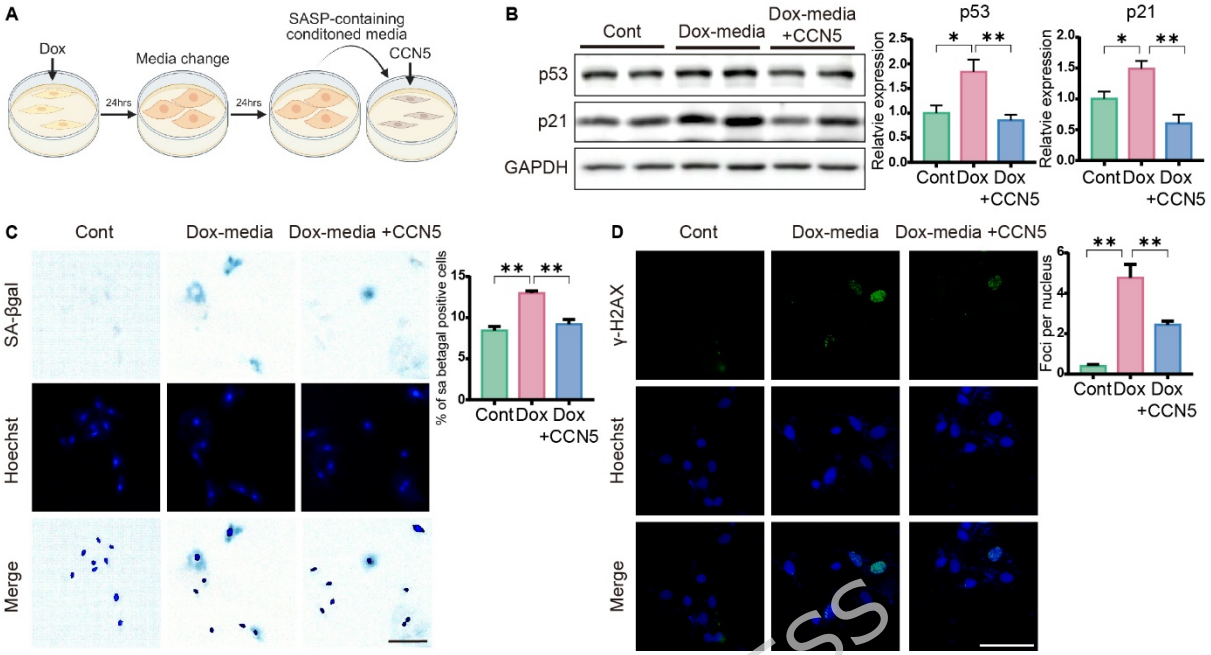

Fig. 5. CCN5 restores apoptotic responses in senescent H9c2 cardiac myoblasts and fibroblasts.

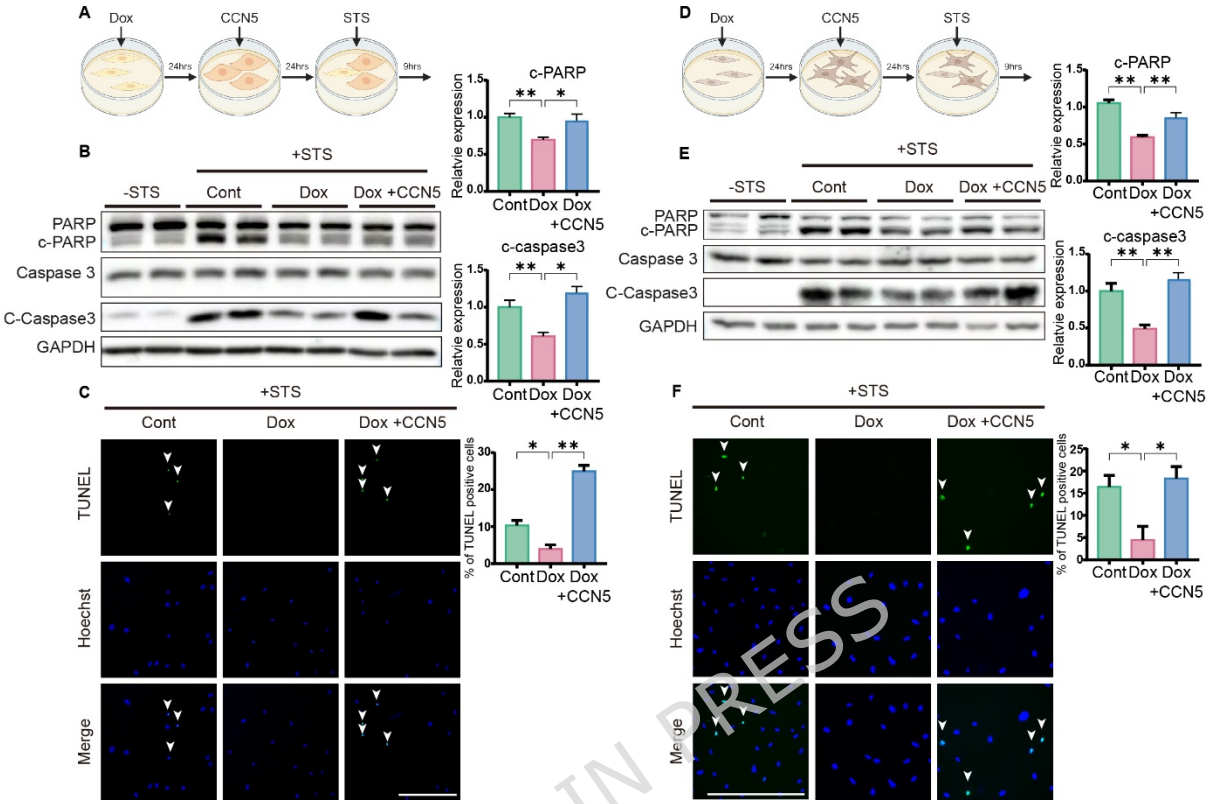

Fig. 6. CCN5 inhibits senescence in an *in vivo* mouse heart model.